Phonons in CdTe-HgTe superlattices

1998 J. Phys.: Condens. Matter 10 3177

(http://iopscience.iop.org/0953-8984/10/14/007)

J. Phys.: Condens. Matter **10** (1998) 3177–3193. Printed in the UK PII: S0953-8984(98)85978-X

Phonons in CdTe–HgTe superlattices

B D Rajput and D A Browne†

Department of Physics and Astronomy, Louisiana State University, Baton Rouge, LA 70803, USA

Received 14 July 1997, in final form 9 December 1997

Abstract. We present a lattice dynamics study of CdTe–HgTe superlattices grown along the (001) and (111) directions within the framework of the adiabatic bond charge model. We find that the long-range Coulomb interaction between particles situated on the opposite sides of the interface needs to be handled carefully to get sensible frequencies and eigenvectors with the proper symmetry and continuity. CdTe–HgTe superlattices grown along the (001) direction show many propagating modes that travel with different wavevectors in CdTe and HgTe layers. The wavevector in HgTe differs from the bulk value, particularly at long wavelengths. For (111) superlattices all of the optical modes are either confined or interface modes. In both cases, the frequencies of the HgTe optical modes do not map well to the bulk LO branch, and the highest HgTe LO mode consistently remains below the bulk value even for 27 layers of HgTe. Our results indicate that all of the unidentified peaks seen in the Raman spectra of (001) superlattices can be explained in terms of superlattice modes.

1. Introduction

The lattice dynamics of semiconductor superlattices has attracted a lot of attention in recent years [1]. Because of the reduced symmetry and additional periodicity of these structures, many new zone-centre optical modes are created, which can be divided into *propagating*, *confined* and *interface* modes. Propagating modes extend throughout the superlattice whereas confined modes have appreciable amplitude in one material and decay exponentially in the other. Interface modes are localized at or near the interface. The propagating and confined modes are derived from the optical and acoustic branches of the two bulk materials, while interface modes lie in the band gaps of the two materials. A number of Raman studies [2–5] have observed these modes near the zone centre. Various theoretical models [3, 5–11] of varying complexity have been used to study these modes.

The vast majority of the work on unstrained superlattices has studied AlAs–GaAs and GaAs–$Ga_xAl_{1-x}As$ superlattices. Comparatively little attention has been paid to understanding the vibrational properties of other lattice-matched systems such as CdTe–HgTe. Since the proposal [12] in 1979 of CdTe–HgTe superlattices as a new material for infrared optoelectronics, a lot of effort [13] has been devoted to understanding the optical and electronic properties of this structure. However, only two Raman studies of the phonon properties have appeared in the literature. The first study [14] reported the observation of CdTe optical phonons in the resonant Raman scattering studies of CdTe–HgTe superlattices grown along the (111) direction, while the other [15] observed mostly HgTe optical phonons along with some unidentified peaks in the Raman spectra of (001) superlattices. There is

† Email address: browne@rouge.phys.lsu.edu.

0953-8984/98/143177+17$19.50

as yet no comprehensive theoretical examination of the lattice dynamics of CdTe–HgTe superlattices, although one study [16] devoted to the phonon density of states of the surfaces and single interfaces of the CdTe/HgTe system has appeared. However, the phonon density of states does not provide any information about the individual modes that can be compared directly with the results of Raman scattering experiments. Moreover, the system consisting of a single interface between two semi-infinite slabs is fundamentally different from the periodic structure of a superlattice and the phonon spectrum of the former lacks many features that arise purely from the periodicity of the superlattice.

From the point of view of lattice dynamics, the CdTe–HgTe superlattice is different from that of GaAs–AlAs in two important ways. Both GaAs and AlAs are semiconductors, with similar phonon properties. In fact, the *ab initio* phonon force constants calculated for GaAs give [17] an accurate description of the phonon dispersion of AlAs. As a result of this similarity in the structural and dynamical properties of the two materials, the mass approximation, in which the dynamical matrix of AlAs is obtained from that of GaAs by changing the cation mass only, has been quite popular in studies [5, 8] of GaAs–AlAs superlattices. This completely rules out the proper modelling of the interface between the two materials. Even when different force constants were used [11], the interface was modelled in a rather *ad hoc* fashion by averaging both the short-range and the long-range force constants at the interface.

In contrast to those of GaAs–AlAs systems, the constituents of the CdTe–HgTe superlattice are qualitatively very different materials. CdTe is an ordinary semiconductor whereas HgTe is a zero-gap semi-metal. Though both materials are partly covalent, the semi-metallic nature of HgTe leads to a charge density that is much less localized than in CdTe. Therefore, the casual treatment of the modelling of the interface using the average of the properties of each material that is common in treatments of GaAs–AlAs superlattices does not give sensible answers for CdTe–HgTe superlattices.

An examination of the phonon dispersion of HgTe and CdTe shows that, unlike those of GaAs and AlAs, the optical branches of CdTe and HgTe overlap significantly. As a result, CdTe–HgTe superlattices will allow optical modes that can propagate in both materials. Such modes, since they do not exist in GaAs–AlAs, have not been given much attention. They have been observed in Raman studies [18] of GaAs–$Ga_{1-x}Al_xAs$, since for $x < 1$ GaAs and $Ga_{1-x}Al_xAs$ have partially overlapping optical branches. However, the alloy nature of $Ga_{1-x}Al_xAs$ makes theoretical studies difficult. Because of the overlap in the optical branches of CdTe and HgTe, the CdTe–HgTe superlattice will have all three kinds of optical phonons, providing us with a lattice-matched system with partially overlapping optical bands without the complications of a disordered alloy.

The apparently contradictory results of the two [14, 15] Raman studies of CdTe–HgTe superlattices mentioned above remain unexplained. While a lattice dynamical study alone will not explain why CdTe modes are seen in one case and HgTe modes in the other, it will provide the necessary groundwork for a complete study of Raman activity and might provide an explanation for the unidentified peaks in the Raman spectra seen in reference [15].

In this paper we present a study of the phonon properties of CdTe–HgTe superlattices within the framework of the adiabatic bond charge model. Phenomenological models, though less fundamental than the density functional approach, seem to be the only feasible approach to studying phonon properties of complex systems such as superlattices, which have large unit cells, and disordered alloys. For CdTe–HgTe superlattices in particular, density functional approaches are hampered by the overlap of the conduction bands of HgTe with the valence bands of CdTe and by the necessity to account for the very strong spin–orbit coupling present in any total energy or Baroni-type [19] calculation. Also, since

non-local pseudopotential calculations [20] are necessary to reproduce the electronic density, the usual local density approximation may not be adequate. Since our model can reproduce [21] the bulk phonon properties, the real usefulness of a density functional calculation would be to give *a priori* values for the model parameters, particularly at the interface.

Our choice of the adiabatic bond charge model was dictated by a desire to have as few adjustable parameters as possible. Traditionally, the lattice dynamics of II–VI materials with zinc-blende crystal structure has been treated using rigid-ion or shell models [22, 23]. These models give good fits to the observed phonon dispersion curves at the cost of a large number of adjustable parameters (ten or more), some of which have no physical interpretation. The adiabatic bond charge model, which is based on the first-principles studies of the electronic structure of covalent materials, has been applied with great success to group IV elements [24], III–V compounds [25] and GaAs–AlAs superlattices [6, 11]. In this model the valence electron charge density is represented by massless point particles, the bond charges (BCs), that are placed along the line joining the two ions and follow the ionic motion adiabatically. These bond charges interact with each other and with the ions through short-range potentials and the screened Coulomb interaction. By accounting for the valence electron screening, the six-parameter adiabatic bond charge model gives results that show better agreement with the neutron scattering data than rigid-ion or shell models.

This model was long believed to be unsuitable for II–VI compounds because of their highly ionic character. However, we recently showed [21] that the six-parameter adiabatic bond charge model provides a good description of the lattice dynamics of bulk II–VI semiconductors and semi-metals with a zinc-blende structure (CdTe, ZnS, ZnSe, ZnTe, HgSe and HgTe), provided that the bond charges are placed at positions predicted by the non-local pseudopotential studies [20] of the valence electron charge density. The agreement with experimental data was as good as with other lattice dynamical models requiring ten or more parameters. We therefore believe this model to be a good starting point for discussing the properties of II–VI superlattices.

The rest of the paper is organized as follows. Section 2 is devoted to the method of calculation and how the very different Coulomb interactions in the two materials are handled. In section 3 we present our results for various CdTe–HgTe superlattices grown along the (001) and (111) directions and in section 4 we compare our results for (001) superlattices with the existing Raman scattering data. Finally, section 5 gives a brief summary and conclusion.

Table 1. BCM force constants for CdTe and HgTe in units of e^2/v_a, where v_a is the unit-cell volume.

	$\phi''_{ii}/3$	$\phi''_1/3$	$\phi''_2/3$	B_1	B_2	Z^2/ϵ	Z
CdTe	6.85	0.77	23.34	0.39	15.44	0.1830	1.15[a]
HgTe	6.46	0.081	13.46	1.08	15.60	0.1062	1.03[a]

[a] ϵ_∞ for CdTe was taken from reference [34] and for HgTe from reference [35].

2. Method of calculation

In the bond charge model, the short-range interactions describe a direct interaction ϕ''_{ii} between the anion and cation, an interaction between a bond charge and its adjacent cation (ϕ''_1) or anion (ϕ''_2), and a three body BC–ion–BC Keating potential B_1 and B_2 for each ion. In addition, one accounts for the long–ranged Coulomb interactions (Z^2/ϵ) of the

anion, the cation and the bond charges. The difference in the electronic structure of CdTe and HgTe is reflected in their BCM parameters [21], shown in table 1, in the fact that the ion–BC parameters $\phi_1''/3$, $\phi_2''/3$ and the Coulomb interaction parameter Z^2/ϵ for HgTe are considerably smaller than those for CdTe. In particular, the Coulomb parameter for CdTe is almost twice as large, resulting in a large mismatch in the Madelung energy of the two materials.

Therefore the parameters describing the interface must be chosen carefully. Instead of taking *ad hoc* averages, we have tried to incorporate, at a microscopic level, the macroscopic boundary conditions of uniform stress and uniform electric potential at the interface. The parameters for the short-range interactions between particles located on the same side of the interface were taken to be corresponding bulk values except the force constants between the interfacial ions and the bond charges surrounding them on either side, which were taken to be the averages of the corresponding parameters for the two materials. Also, the parameters for BC–BC interactions surrounding the interfacial ions were taken to be the averages of the corresponding bulk values. The net effect of using these approximations is to produce a uniform local environment on both sides of the interfacial ion.

Because of the large mismatch in the Madelung energies of the two materials, fixing the Coulomb parameter Z^2/ϵ was not so simple. Simple recipes, namely, assigning the uniform value of $(Z^2/\epsilon)_{\text{ave}} = (Z^2/\epsilon)_1 + (Z^2/\epsilon)_2$ to every particle in the superlattice, or using respective bulk values for particles on the same side of the interface and $(Z^2/\epsilon)_{\text{ave}}$ for those on the opposite sides, yield imaginary frequencies.

A better solution is to treat the two materials as two media with different dielectric constants. For a point charge in a semi-infinite medium with dielectric constant ϵ_1, adjacent to a second semi-infinite dielectric medium with dielectric constant ϵ_2 the potential on the same side of the interface is given by $Z/(\epsilon_1 r)$ plus a small correction proportional to $(\epsilon_2 - \epsilon_1)/(\epsilon_2 + \epsilon_1)$ [26]. The potential on the other side of the interface is $Z/(\epsilon_{\text{ave}} r)$, where $\epsilon_{\text{ave}} = (\epsilon_1 + \epsilon_2)/2$. Therefore, in our calculation the Coulomb interaction for two charges on the same side of the interface was divided by the corresponding bulk dielectric constant while the Coulomb interaction for charges on different sides or charges on the interface was divided by ϵ_{ave}. The particles in the superlattice were assigned the same charges as in the corresponding bulk materials except for interfacial ions for which we found it necessary to use $(Z_{\text{CdTe}} + Z_{\text{HgTe}})$ in the case of a (001) superlattice. With this charge assignment, the bulk unit cells containing the interfacial ions at the two interfaces are not charge neutral, although overall neutrality of the superlattice unit cell is preserved. This interfacial modelling works for both (001) and (111) superlattices and gives positive eigenvalues reflecting the required symmetry of the problem and eigenvectors that are continuous at the interfaces.

The superlattice modes and frequencies are calculated by solving the standard BCM equations [21] for the SL unit cell. The short-range part of the dynamical matrix was constructed explicitly by unfolding the FCC lattice along the growth direction. The Coulomb part was calculated by using the layered method [9] as well as the conventional Ewald method. In order to use the layered method for the (111) superlattice one has to work in a rotated space in which the x-, y-, z-directions correspond to $(1\bar{1}0)$, $(11\bar{2})$ and (111) respectively. For the conventional Ewald method, the superlattice direct-lattice vectors are (l_1, l_2, l_3) where l_1, l_2 and l_3 are integers such that $l_1 + l_2 + Nl_3$ is even for a (001) superlattice and $l_1 + l_2 + l_3$ is a multiple of $2N$ for a (111) superlattice, N being the number of layers in the superlattice unit cell. The reciprocal vectors can be obtained by choosing one of the bulk FCC primitive reciprocal-lattice vectors along the growth direction and then folding it N times.

3. Results and discussion

As can be seen in figure 1 of reference [21], the optical bands of CdTe and HgTe overlap partially. In fact, almost the entire LO branch of HgTe overlaps with the corresponding CdTe mode. Moreover, the highest acoustic frequency in CdTe is higher than the smallest optical frequency in HgTe. Because of this, the phonon dispersion of CdTe–HgTe superlattices consists of closely spaced optical bands. There is no clear-cut separation between the bands derived from CdTe or HgTe optical branches except for the few highest branches, which are derived from CdTe optical phonons. Therefore, the identification of SL modes in terms of CdTe or HgTe modes had to be done by examining the eigenvectors.

A classification based only on the atomic displacement can be misleading because of the large mass difference in Cd and Hg. Instead, we use a criterion based on the mean squared momentum in each material. This has the advantage of more directly measuring the energy stored in each material, and is also directly related to the dipole oscillator strength in the optical adsorption. We thus define the *vibrational strength* of the mode j by

$$S_j = \sum_{\kappa=0}^{N-1} |m_\kappa \boldsymbol{u}_\kappa|^2 = S_j^{\mathrm{CdTe}} + S_j^{\mathrm{HgTe}}. \tag{1}$$

Superlattice modes with $S_j^{\mathrm{M}} \geqslant cS_j$ where $c = 0.8$ were classified as modes of material M. All other modes were classified as extended modes. Too large a value of c will classify confined modes that have non-negligible penetration into the other layer as extended modes, while a low value of c ($\sim$0.5) will result in most modes being classified as confined modes. The number 0.8 was found to be an appropriate compromise.

With this classification scheme in mind, we will now analyse the dispersion curves of CdTe–HgTe superlattices grown along the (001) and (111) directions. For convenience in the following discussion, we will use SL as a shorthand notation for superlattice, (m, n)SL001 for an (m, n) layer superlattice along the (001) direction and (m, n)SL111 for a superlattice grown along the (111) direction.

3.1. (001) superlattices

In figure 1 we present the phonon dispersion for (5, 5)SL001. A complicated pattern is seen when the wavevector is in a plane perpendicular to the growth direction. The bands with frequencies lower than 3.46 THz are derived from the acoustic branches and the bands with frequencies between 2.66 THz and 3.46 THz are derived solely from the CdTe acoustic branches.

The phonon dispersion for $\boldsymbol{q}$ along the growth direction consists of a series of lines with no or linear dispersion. The high-frequency branches with no dispersion are the confined optical phonons while the low-frequency branches with linear dispersion are the folded acoustic phonons. This is similar to the case for GaAs–AlAs superlattices except that one can find optical branches which have linear dispersion and therefore look like folded acoustic branches. These dispersive branches represent optical frequencies which are allowed in both materials, and are absent in the (111) superlattices discussed later since the bulk LO branches in that direction do not overlap. In the (001) direction, the exact positions at which they appear depend on the thickness of the superlattice, but generally they appear in the overlapping region of the bulk LO branches. While these modes appear to have been obtained by the folding of the LO branch of HgTe, they are not folded in the usual sense of the word since neither their frequencies nor their displacement patterns can be accounted for in terms of a superlattice wavevector $Q = l\pi/d$, l being an integer and

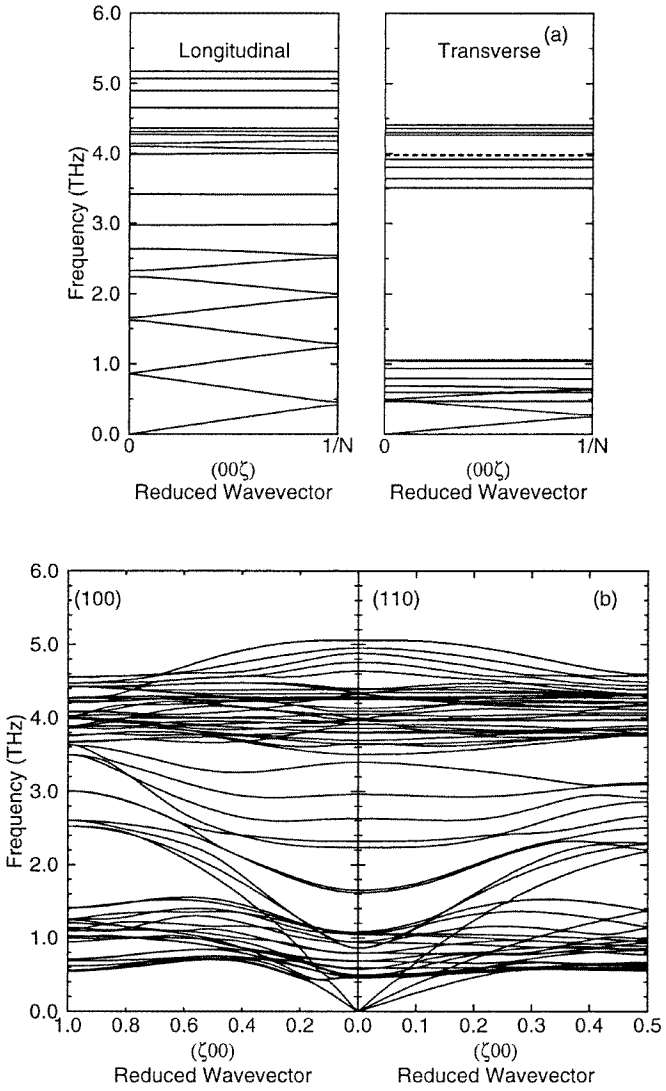

Figure 1. Phonon spectra of (5, 5)SL001 (a) parallel and (b) perpendicular the growth direction. The dashed line in the transverse panel indicates two closely spaced TO modes, one of which is an interface mode (lower branch). The reduced wavevector is in units of $2\pi/a$, where a is the bulk lattice constant.

$d = d_1 + d_2$ being the superlattice period. This is because these modes propagate at different wavevectors in the two layers. Therefore it is more appropriate to call them dispersive or propagating phonons. These modes propagate with comparable amplitudes in the two layers and have complex amplitude modulation, as figure 2 shows. The wavevector assignment for these modes was done by looking at their displacement patterns in the two layers. Many of these modes have wavevectors of the form $(l + 0.5)\pi/d_i$, where l is an integer and d_i is the layer thickness. This is precisely the condition for an antinode at the interface, which is what is observed in the displacement patterns of these modes. We find that for a given mode the wavevector in the CdTe layers is very close to the value at which the particular

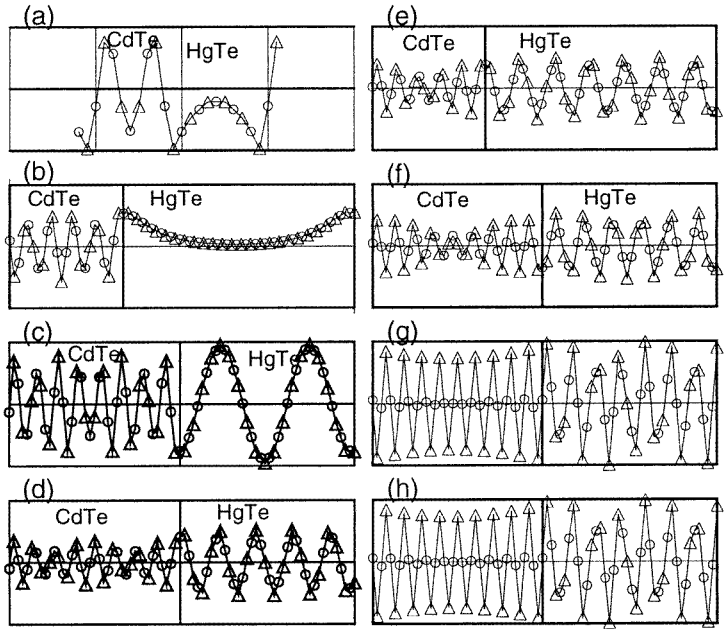

Figure 2. Displacements for the extended LO modes. Circles denote cation displacements and triangles denote anion displacements. The solid curves are a guide to the eye. The frequency of the modes decreases from (a) to (h).

mode is allowed in bulk CdTe. However, the wavevectors in HgTe layers are different from the corresponding bulk values. For example, the mode with $f = 4.305$ THz in figure 2(c) is allowed in bulk HgTe at $\zeta \simeq 0.31$, where ζ is the reduced wavevector. A look at the displacement pattern shows that $\zeta \simeq 0.2$ in the superlattice, significantly different from the bulk value. This difference decreases as ζ approaches the zone boundary.

For folded acoustic branches, which are generally explained in terms of Rytov's [27] elastic continuum model, we get slopes of 2.816 cm s^{-1} and 2.717 cm s^{-1} for the zeroth- and the first-order LA curves in the dispersion of (5, 5)SL001, as compared to 2.912 cm s^{-1} predicted by Rytov's model. The slopes of the higher-order LA modes depart significantly (2.31 cm s^{-1} for the second folded LA), mainly because of the fact that these branches are folded from regions of the bulk Brillouin zone where the bulk LA branches of the two materials do not exhibit linear dispersion. The agreement with Rytov's model for the folded TA modes is even worse because of the flattening of bulk TA branches.

An examination of the frequencies and eigenvectors of the modes in various superlattices shows that not all of the zone-centre SL modes can be identified as bulk CdTe or HgTe modes. Figure 2(a) shows that modes lying above the bulk LO frequency of HgTe, and thus forbidden in bulk HgTe, are not necessarily confined in CdTe layers and may have significant momentum in HgTe layers. Similarly, figure 2(b) shows that modes lying below the bulk LO frequency of HgTe are not necessarily propagating modes in HgTe layers. As mentioned above, we identified modes by calculating their vibrational strengths using equation (1). For (5, 5)SL001, out of the ten LO modes only four modes could be identified as CdTe LO modes and four as HgTe LO modes. The remaining two fell under the category of extended modes. The first of these, at 4.35 THz, has a frequency which is slightly higher than the bulk LO frequency of HgTe but never completely decays in HgTe layers, as figure 2(a)

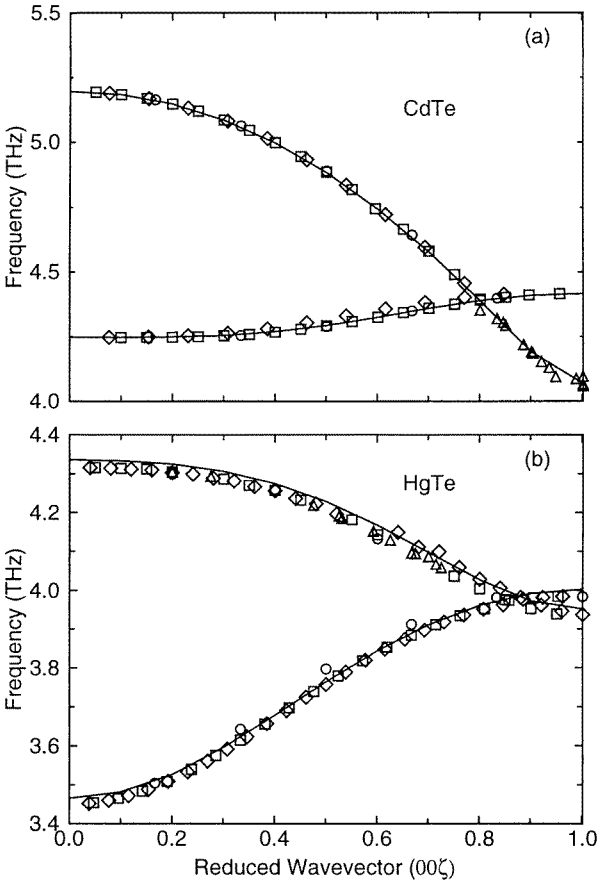

Figure 3. Mapping of the (001)SL modes to the bulk modes (——) of (a) CdTe and (b) HgTe. The confined modes are ○: (5, 5)SL001, ◇: (12, 25)SL001 and □: (19, 20)SL001, and △ indicates an extended mode.

shows. In fact, the vibrational strength of this mode is almost equally divided between the two layers. The other mode (4.09 THz) is allowed in both materials and shows oscillatory behaviour in both layers.

Because of the non-overlapping TO branches of CdTe and HgTe, the superlattice TO modes show more confinement and all of the modes can be identified as bulk or interface modes. In the bulk HgTe TO range one finds a single additional TO mode that is an interfacial mode with most of its energy in the HgTe layer. There is correspondingly one mode missing from the bulk CdTe TO range.

The SL modes confined to either layer are generally related to the bulk optical phonons of constituent materials by defining an effective wavevector in analogy with the problem of a particle confined in a box:

$$k_n = \frac{n\pi}{(N+\gamma)d} \qquad n = 1, 2, \ldots, N \tag{2}$$

with N being the number of monolayers in the slab and d the thickness of the monolayer. The parameter γ is a measure of the degree of confinement of the mode, $\gamma = 0$ implying

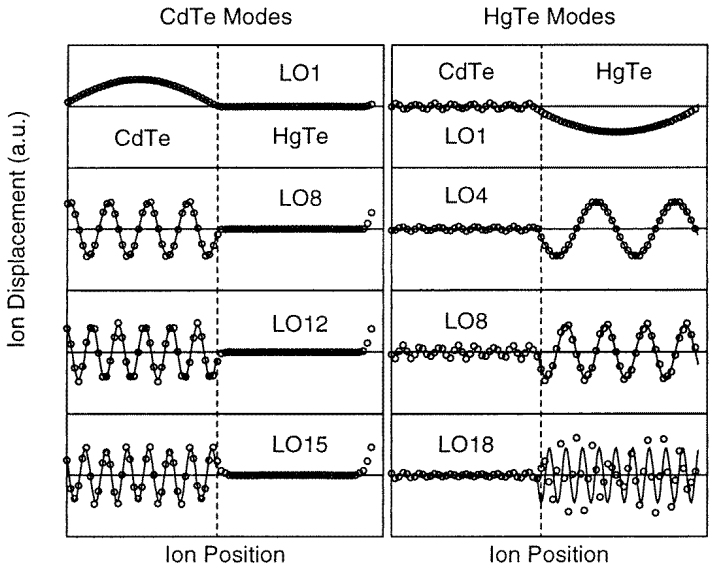

Figure 4. Displacements for the LO modes in (19, 20)SL001. The envelopes are sine or cosine curves normalized to the appropriate vibrational strength.

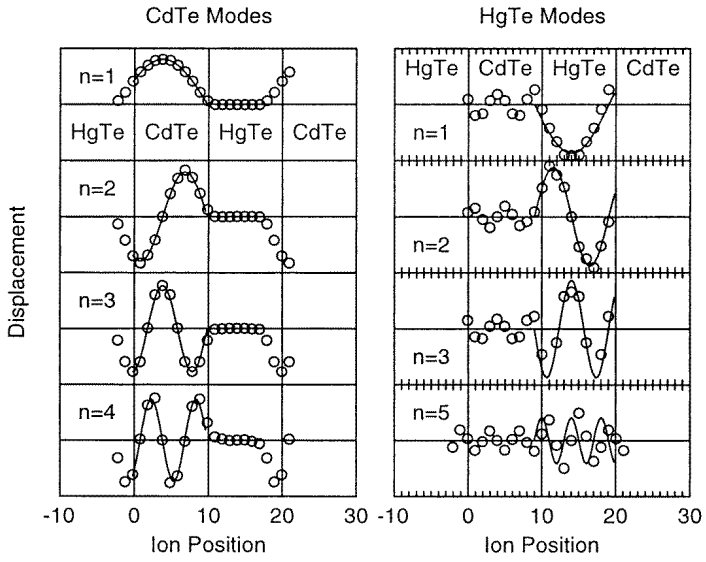

Figure 5. Displacements for the LO modes in (5, 5)SL001. The envelopes are sine or cosine curves normalized to the appropriate vibrational strength.

perfect confinement. The value of γ is model and mode dependent and is generally between 0 and 1 for GaAs and AlAs [5, 8, 9, 10, 28].

The choice of $\gamma = 1$ for the CdTe optical modes gives a very good mapping of the SL zone-centre modes onto the bulk dispersion of CdTe along the (001) direction (figure 3(a)), and results in a fair mapping for HgTe TO modes, especially for

the thicker superlattice (figure 3(b)). However, for the LO modes the best mapping, which was still worse than that for TO modes, came from choosing $\gamma = 0$. The wavevector assignments shown in these figures also give the best envelope for ionic displacements.

We have also plotted the extended modes along with the confined modes on the bulk dispersion of CdTe and HgTe in figure 3. Like the confined CdTe modes, these extended modes map quite well to the bulk dispersion curves of CdTe. However, mapping to the bulk HgTe dispersion follows the pattern shown by the confined HgTe modes.

An analysis [29] of the thickness dependence of the highest LO modes shows that, as in GaAs–AlAs SLs, the frequencies of highest CdTe and HgTe LO modes increase with increasing thickness of the respective layer. The CdTe mode frequency approaches the bulk LO value for a layer thickness of 19 monolayers or 61.5 Å, as compared to 30 Å or roughly 11 monolayers for GaAs or AlAs [30]. The highest HgTe LO mode remains slightly, though distinctly, below the bulk value even when the HgTe layer is 25 monolayers (81 Å) thick.

This trend, when combined with our inability to properly map HgTe LO modes in the superlattice onto the bulk LO curve suggests that the frequencies of HgTe modes in CdTe–HgTe superlattices are lower than the frequencies in bulk HgTe. It can be seen that most of these modes lie consistently below the bulk LO curve. Moreover, figure 2(b) shows that the highest LO mode in the bulk LO range of HgTe is not necessarily a propagating mode.

These observations can be understood in terms of the stronger electric field in HgTe layers due to the presence of higher charges in CdTe layers, which shifts the bulk HgTe frequencies down. While higher charges in CdTe layers tend to lower the frequencies, the lighter cation mass in CdTe layers will tend to push the frequencies up. However, it appears that the perturbation due to the change in the Coulomb parameter is dominant since most of the SL modes lie below the bulk branches. In particular, all of the SL modes up to $\zeta = 0.6$ lie below the bulk dispersion curves. A close examination of figure 3(a) supports the above explanation as most of the confined CdTe modes lie slightly above the bulk curves. However, the effect is not as pronounced as in the case of HgTe.

Figures 4 and 5 give the mass-weighted displacements of the various modes discussed above. Here the anion displacement has been multiplied by -1. The order n of the mode is defined by the number of half-waves in the layer. The envelope shown is a sine (odd-n) or cosine (even-n) curve with the wavevector given by equation (2). To account for the fact that CdTe or HgTe modes are not perfectly confined in their respective layers, we normalized these curves to the vibrational strengths of these modes calculated using equation (1). It can be seen that these envelopes provide an excellent approximation for the displacement patterns of the highest few modes. However, these modes become less confined as the frequency decreases and the cation and anion displacements develop a phase shift. This phase shift is more pronounced for the TO modes [29].

Unlike the confined CdTe modes, which show rapid decay in the HgTe layers, the displacements for the confined HgTe modes show oscillations in the CdTe layers as seen in figures 4 and 5. This behaviour is independent of the thickness of the HgTe layers as similar patterns are seen for (5, 5)SL001 as well as (19, 20)SL001. Also, the displacements of the HgTe modes in (5, 5)SL001 are poorly described by harmonic envelopes, especially for higher n.

The confined HgTe modes of higher order n show oscillations whose amplitudes have modulations characterized roughly by a wavevector $q = l\pi/d$, where d is the thickness of the confining layer. Figure 6 shows displacements in the HgTe layers for many higher-order confined HgTe modes of (19, 20)SL001, all of which lie below the smallest CdTe LO frequency. A harmonic modulation with a period $d = 20$ can be easily observed. Such modes are not seen in GaAs–AlAs system since GaAs (AlAs) does not support harmonic

oscillations at optical frequencies characteristic of AlAs (GaAs), which is a prerequisite for this behaviour. In all four modes most of the momentum is carried by Te ions. In particular, Hg ions hardly move in the LO19 mode, which propagates with a bulk wavevector that is very close to the zone boundary. This is consistent with the BCM prediction of the bulk LO eigenvector for HgTe at the X point of the bulk Brillouin zone [21]. Similar behaviour is seen for modes propagating in CdTe layers with wavevectors close to the bulk X point, as shown in figures 2(g) and 2(h).

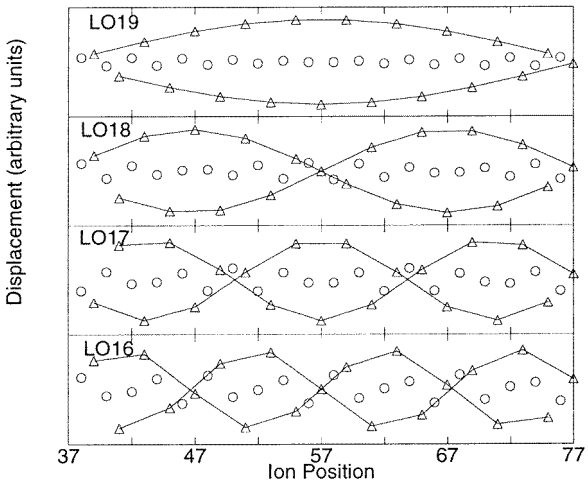

Figure 6. Displacements for the low HgTe LO modes in (19, 20)SL001. Circles denote cation displacements and triangles denote anion displacements. The solid curves are a guide to the eye.

Comparing the dispersion curves along different wavevector directions for the same superlattice, we see that, for the highest optical mode, the frequencies are distinctly different for $\boldsymbol{q} \rightarrow 0$ from the growth direction and from an in-plane direction. Other modes also show this anisotropy but it is more pronounced for the highest modes of the two materials. This anisotropy of the optical phonons has been observed in many Raman studies [4, 31] of GaAs–AlAs superlattices. A detailed analysis [29] of the angular dependence of the zone-centre SL modes, as the wavevector is rotated from the growth direction to an in-plane direction, yields results that are qualitatively similar to those for GaAs–AlAs superlattices. In particular, one can identify many Fuchs–Kliewer [32] modes, which have been observed [33] in GaAs–AlGaAs SLs. All TO modes split as the wavevector rotates from the growth direction to an in-plane direction.

3.2. (111) superlattices

The optical bands of bulk CdTe and HgTe do not overlap in the (111) direction. Therefore the situation is qualitatively similar to that for GaAs–AlAs superlattices and the phonon spectra of CdTe–HgTe superlattices grown along this direction do not contain any propagating optical phonons. In figure 7 we present phonon spectra for (5, 5)SL111. We find that the bands with frequencies between 2.36 THz and 3.22 THz result only from the acoustic branches of CdTe.

A comparison with the spectra for (001) superlattices in figure 1 shows that the

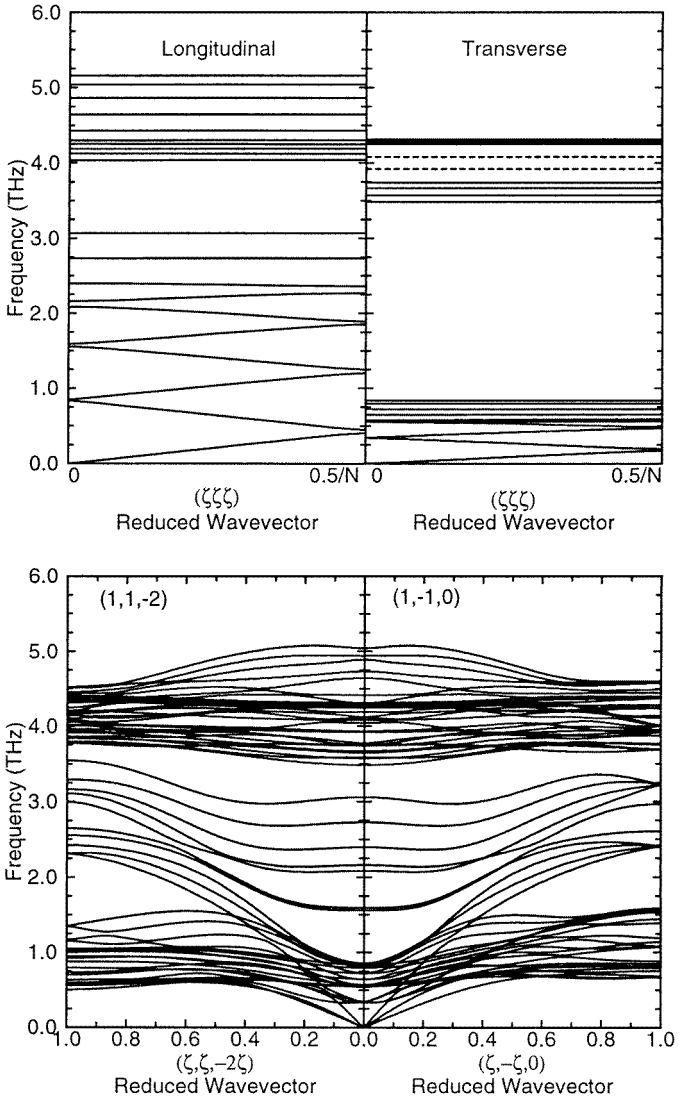

Figure 7. Phonon spectra of (5, 5)SL111 parallel and perpendicular to the growth direction. The dashed lines indicate the transverse interface modes discussed in the text. The reduced wavevector is in units of $2\pi/a$, where a is the bulk lattice constant.

dispersion curves for (001) and (111) superlattices are quite different even for superlattices with the same number of layers. This is most obvious near $\boldsymbol{q} = 0$ where, because of the zone-folding effects, different modes are seen in the two superlattices. This can be easily seen in the acoustic frequency regime. Furthermore, the frequency of the highest optical mode is slightly less in (111) superlattices than in (001) superlattices. In the confined-phonon picture, this can be understood in terms of the larger dispersion of the LO branch in the (111) direction.

For these superlattices, all of the optical modes propagating along the growth direction can be identified as confined or interface modes. In particular, all the LO modes can be

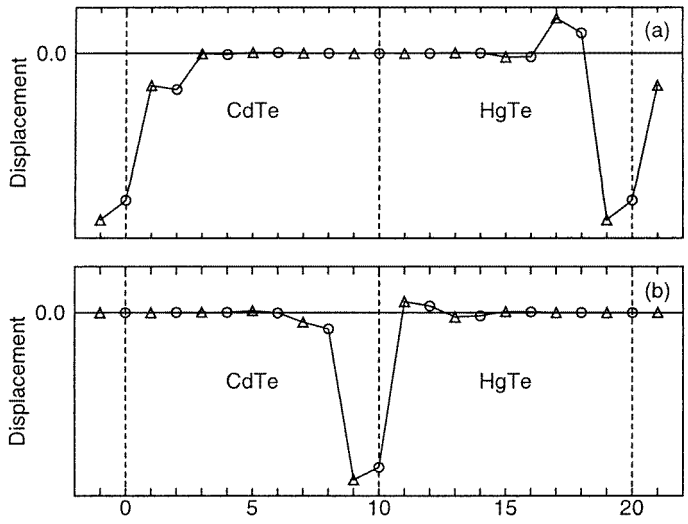

Figure 8. The two interface modes, each doubly degenerate, in a (5, 5)SL. The dotted lines denote the location of the interfacial Te ion. The frequencies are (a) 4.08 THz and (b) 3.92 THz. These modes are seen in all (111) superlattices.

identified as confined CdTe or HgTe modes. The phonon dispersion of this superlattice has two TO modes each doubly degenerate, at 4.08 THz and 3.92 THz, that lie in the band gaps of the two materials (dashed lines in figure 7) and therefore are true interface modes, highly localized at the two interfaces as shown in figure 8. These modes show no dispersion at all and appear in the spectra of all of the superlattices that we considered. All other TO modes are confined modes.

In figure 9 we present the mapping of superlattice modes to the optical phonon dispersion of bulk CdTe and HgTe respectively. As in the (001) superlattices, we find that $\gamma = 0$ for LO modes and $\gamma = 1$ for TO modes. However for the (5, 5)SL111 LO branch we got better mapping with $\gamma = 1$. Due to their better confinement, the overall mapping for HgTe modes is better than for the (001) superlattices, although the long-wavelength modes still lie below the bulk curves. Also, the frequency of the highest HgTe LO mode remains below the bulk LO frequency even for a (10, 27)SL111 [29], indicating that the lowering of long-wavelength HgTe frequencies seen in (001) superlattices is not dependent on the growth direction.

The angular dispersion results for (111) SLs are qualitatively similar to those for the (001) superlattices [29]. One can identify many slab-like modes when the wavevector is along $(1\bar{1}0)$. In particular, the two degenerate interface modes split for wavevectors not parallel to the growth direction.

4. Comparison with experiments

So far, only two Raman scattering studies [14, 15] of CdTe–HgTe superlattices have been reported in the literature. In the first of these, photoluminescence and resonant Raman scattering measurements were performed [14] on superlattices grown along the (111) direction. The Stokes spectra of these experiments showed sharp lines at energies corresponding to the bulk CdTe LO phonon and its higher-order harmonics in addition

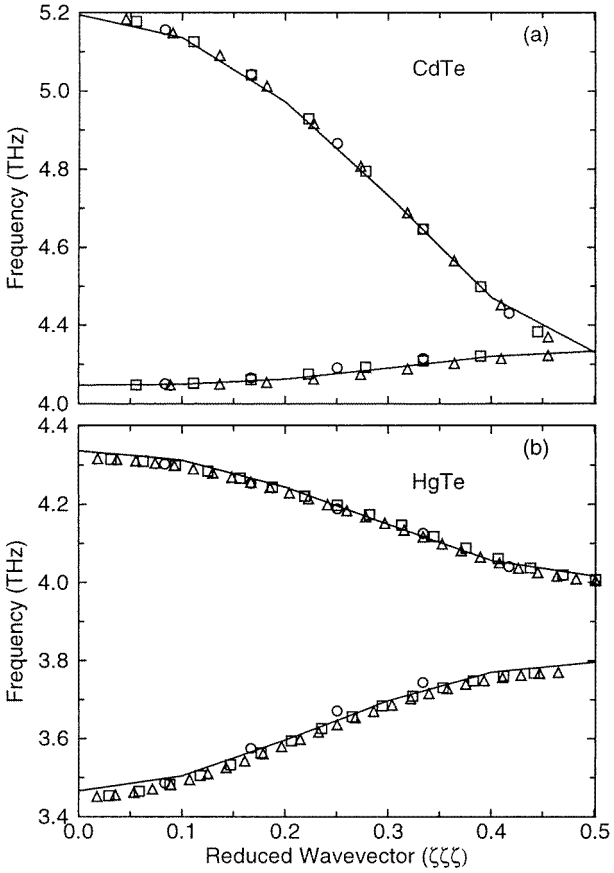

Figure 9. Mapping of (111) superlattice modes to the bulk dispersion (——) of (a) CdTe and (b) HgTe. Key to the symbols: ○: (5, 5)SL111; □: (8, 16)SL111; △: (10, 27)SL111.

to photoluminescence backgrounds. Since the main focus of the study was the electronic properties of CdTe–HgTe superlattices, the only interesting lattice dynamics result noted was the absence of peaks in the Raman spectra corresponding to any of the HgTe phonons or any other CdTe phonons. The three superlattices SL1, SL2 and SL3 investigated in reference [14] correspond to (8, 16)SL111, (10, 27)SL111 and (5, 10)SL111, respectively. The first two superlattices were discussed earlier and it was shown that all of the optical modes are well confined in their respective layers and can be described by means of an effective wavevector. The results for the third superlattice are qualitatively similar to those for the other two.

The second study was done by Feng *et al* [15] who performed Raman scattering experiments on (001) superlattices. In these structures, the CdTe layer actually contained a small amount of Hg and so these were actually $Cd_{1-x}Hg_xTe$–HgTe superlattices, with $x \simeq 0.15$. $Cd_{1-x}Hg_xTe$ is a mixed alloy and exhibits two-mode behaviour for all values of x. Since we studied CdTe–HgTe superlattices rather than $Cd_{1-x}Hg_xTe$–HgTe, we will not get the two-mode behaviour and will not see HgTe-like modes associated with the alloy. However, since the value of x is quite small, the CdTe-like modes of $Cd_{1-x}Hg_xTe$ are expected to be quite close to the optical frequencies of CdTe [23] and our theoretical results

should agree with the experimental results [15].

The superlattices SL1 and SL2 considered in reference [15] correspond to (19, 20)SL001 and (12, 25)SL001 respectively. Many properties of these structures were discussed above. Here we focus our attention on the identification of some of the calculated modes with the experimental observations. SL2 had a 300 Å CdTe cap whereas SL1 had no CdTe cap. The experiment was done in the near-back-scattering geometry in which the incident and scattered light waves are parallel to each other and almost perpendicular to the surface of the sample. In this geometry both LO and TO modes are allowed, with LO modes being favoured. Unlike the results of reference [14], the Raman spectra of SL1 showed no peaks corresponding to CdTe phonons. However, there were two peaks, at 155 cm^{-1} and 425 cm^{-1}, which were far from any of the known modes of CdTe or HgTe. The latter peak was actually a broad feature extending from 350 to 550 cm^{-1} with a peak near 425 cm^{-1}. The Raman spectra of the other superlattice SL2, which had a CdTe cap, showed many CdTe optical phonons and one unknown peak at 244 cm^{-1}. That the two superlattices had unknown peaks at different positions suggests that these modes might be SL modes.

In our calculations of these superlattices, we find one CdTe LO mode at 155.46 cm^{-1} (4.664 THz) in the spectrum of SL1. The spectrum of SL2 does not contain any modes close to this energy. Consequently we can attribute the unknown peak at 155 cm^{-1} in the Raman spectrum of SL1 to a superlattice mode since the difference between the former and 155.46 cm^{-1} is well within the resolution (2–3 cm^{-1}) of that experiment.

The identification of the other unknown peak, at 425 cm^{-1} for SL1, to a SL mode is not as straightforward. First of all, it should be realized that this peak, and the peak in SL2's spectrum can be explained only, if at all, in terms of higher harmonics since the optical frequencies of CdTe lie between 127.3 cm^{-1} and 173.2 cm^{-1} and those of HgTe range from 115.3 cm^{-1} to 138 cm^{-1}. For SL1, we find many closely spaced modes near 425 cm^{-1}. For example, there are two HgTe LO modes at 141.86 cm^{-1} and 142.32 cm^{-1} and eight doubly degenerate CdTe TO modes between 141.55 cm^{-1} and 142.6 cm^{-1}. The third harmonic of all of these modes is within the experimental resolution of 425 cm^{-1}. The broad feature at this frequency could be a manifestation of all of these modes or due to HgTe LO modes only, since LO modes are favoured in the near-back-scattering geometry. Similarly, the unknown peak at 244 cm^{-1} in SL2's spectrum can be due to the second harmonic of the HgTe TO at 121.89 cm^{-1} or due to the third harmonic of either of the two HgTe LO modes at 81.73 cm^{-1} and 81.04 cm^{-1}.

5. Summary and conclusion

We have studied phonons in CdTe–HgTe superlattices grown along the (001) and (111) directions. This is the first study of its kind for these structures and therefore we were unable to compare our results with other studies of CdTe–HgTe superlattices. However, wherever possible, we compared our results with existing studies of GaAs–AlAs superlattices. We find that the question of interface modelling, which has been treated casually in the case of GaAs–AlAs superlattices, becomes an important issue and needs to be treated carefully to produce sensible results. In particular, the Coulomb interaction between two particles situated on opposite sides of the interface has to be handled in a physical manner, consistent with the boundary conditions of macroscopic electrostatics.

For superlattices grown along the (001) direction, we see many dispersive LO branches. These branches lie in the overlapping regions of bulk LO branches of CdTe and HgTe and represent phonons propagating in both materials. These modes have different wavevectors in CdTe and HgTe layers that cannot be assigned by using some simple scheme. We assigned

these wavevectors by examining the displacement patterns of these modes. We find that the wavevectors in CdTe layers are close to the corresponding bulk values but the wavevectors in HgTe layers are in general different from the wavevectors of the corresponding bulk HgTe frequencies.

Our results for (111) superlattices are qualitatively similar to those for GaAs–AlAs superlattices. This is because the optical bands of CdTe and HgTe do not overlap in the (111) direction. However, for both the (001) and (111) directions we find that the frequencies of HgTe modes, especially at long wavelengths in the (001) direction, do not map as well to the bulk dispersion of HgTe as do those of CdTe. Furthermore, the frequency of the highest HgTe LO mode does not attain the bulk limit even for a 27-monolayer-thick HgTe layer. Such an effect is not seen in GaAs–AlAs superlattices where one can always map the calculated and even the experimentally determined SL modes to appropriate bulk branches. We attribute this to the substantial differences in the dielectric properties of the two materials, which result in a stronger electric field because of the higher Coulomb parameter in CdTe layers.

Since the frequency shifts are small, one can always wonder whether these effects are an artifact of the model. This question can be addressed experimentally. A first-principles calculation would be useful as well, and could also shed light on the appropriate parameters to use for the ions at the CdTe/HgTe interface. Since the short-range and long-range parameters of BCM are coupled through the equilibrium conditions, we did not have enough freedom to use different modelling schemes at the interface. Therefore we could not study the dependence of superlattice modes on different interface configurations.

Our work also shows that the unknown peaks in the Raman scattering results of reference [15] can be accounted for in terms of the superlattice modes. The unknown peak at 155 cm^{-1} in the spectra of SL1 can be unambiguously assigned to a confined CdTe LO mode. The other two peaks at 425 cm^{-1} (SL1) and at 244 cm^{-1} (SL2) can be identified as harmonics of predominantly bulk-like CdTe and HgTe modes that are modified by the superlattice. Thus we see that both CdTe and HgTe modes are present in the results of Feng *et al*. However, CdTe modes could not be identified because they are not multiple harmonics of the zone-centre LO mode in bulk CdTe.

Acknowledgment

This work was supported by the National Science Foundation under Grant No DMR–9408634.

References

[1] Klein M V 1986 *IEEE J. Quantum Electron.* **22** 1760
Jusserand B and Cardona M 1989 *Light Scattering in Solids V* ed M Cardona and G Guntherodt (Heidelberg: Springer)
[2] Merz J L, Barker A S Jr and Gossard A C 1977 *Appl. Phys. Lett.* **31** 117
Colvard C, Merlin R, Klein M V and Gossard A C 1980 *Phys. Rev. Lett.* **45** 298
Sood A K, Menendez J, Cardona M and Ploog K 1985 *Phys. Rev. Lett.* **54** 2111
Sood A K, Menendez J, Cardona M and Ploog K 1985 *Phys. Rev. Lett.* **54** 2115
Ishibashi A, Itabashi M, Mori Y, Kaneko K, Kawado S and Watanabe N 1986 *Phys. Rev.* B **33** 2887
Jusserand B, Alexander F, Dubard J and Paquet D 1986 *Phys. Rev.* B **33** 2897
Levi D, Zhang S L, Klein M V, Klem J and Morkoc H 1987 *Phys. Rev.* B **36** 8032
Wang Z P, Jiang D S and Ploog K 1988 *Solid State Commun.* **53** 661
Mowbray D J, Cardona M and Ploog K 1991 *Phys. Rev.* B **43** 1598

Scamarcio G, Haines M, Abstrieter G, Molinari E, Baroni S, Fischer A and Ploog K 1993 *Phys. Rev.* B **47** 1483
[3] Barker A S Jr, Merz J L and Gossard A C 1978 *Phys. Rev.* B **17** 3181
[4] Colvard C, Gant T A, Klein M V, Merlin R, Fischer R, Morkoc H and Gossard A C 1985 *Phys. Rev.* B **31** 2080
[5] Popovic Z V, Trodahl H J, Cardona M, Richter E, Strauch D and Ploog K 1989 *Phys. Rev.* B **40** 1202
Popovic Z V, Cardona M, Richter E, Strauch D, Tapfer L and Ploog K 1989 *Phys. Rev.* B **40** 3040
Popovic Z V, Cardona M, Richter E, Strauch D, Tapfer L and Ploog K 1990 *Phys. Rev.* B **41** 5904
[6] Yip S K and Chang Y C 1984 *Phys. Rev.* B **30** 7037
[7] Babiker M 1986 *J. Phys. C: Solid State Phys.* **19** 683
Toriyama T, Kobayashi N and Horikoshi Y 1986 *Japan. J. Appl. Phys.* **25** 1895
Chu H, Ren S F and Chang Y C 1988 *Phys. Rev.* B **37** 10 746
Huang K and Zhu B F 1988 *Phys. Rev.* B **38** 2183
Akera H and Ando T 1989 *Phys. Rev.* B **40** 2914
Chamberlain M P, Cardona M and Ridley B K 1993 *Phys. Rev.* B **48** 14 356
[8] Richter E and Strauch D 1987 *Solid State Commun.* **64** 867
[9] Ren S F, Chu H and Chang Y C 1988 *Phys. Rev.* B **37** 8899
[10] Tsuchiya T, Akera H and Ando T 1989 *Phys. Rev.* B **39** 6025
[11] Miglio L and Colombo L 1989 *Surf. Sci.* **221** 486
[12] Schulman J N and McGill T C 1979 *Appl. Phys. Lett.* **34** 663
[13] Schulman J N and McGill T C 1981 *Phys. Rev.* B **23** 4149
Bastard G 1982 *Phys. Rev.* B **25** 7584
Chang Y C, Schulman J N, Bastard G, Guldner Y and Voos M 1985 *Phys. Rev.* B **31** 2557
Kinch M A and Goodwin M W 1985 *J. Appl. Phys.* **58** 4455
Myers T, Myers J R, Hoffman C A and Ram-Mohan L R 1992 *Appl. Phys. Lett.* **61** 1814
[14] Olego D J, Faurie P M and Raccah P M 1985 *Phys. Rev. Lett.* **55** 328
[15] Feng Z C, Perkowitz S and Wu O K 1990 *Phys. Rev.* B **41** 6057
[16] Rey-Gonzalez R, Quiroga L and Camacho A 1995 *J. Phys.: Condens. Matter* **7** 1979
[17] Giannozzi P, de Gironcoli S, Pavone P and Baroni S 1991 *Phys. Rev.* B **43** 7231
[18] Jusserand B, Paquet D and Regreny A 1984 *Phys. Rev.* B **30** 6245
[19] Baroni S, Giannozzi P and Testa A 1987 *Phys. Rev. Lett.* **58** 1861
[20] Chelikowski J R and Cohen M L 1976 *Phys. Rev.* B **14** 556
[21] Rajput B D and Browne D A 1996 *Phys. Rev.* B **53** 9052
[22] Rowe J M, Nicklow R M, Price D L and Zanio K 1974 *Phys. Rev.* B **10** 671
Vagelatos N, Wehe D and King J S 1974 *J. Chem. Phys.* **60** 3613
Kunc K, Balkanski M and Nusimovici M A 1975 *Phys. Status Solidi* b **71** 341
[23] Talwar D N and Vandevyer M 1984 *J. Appl. Phys.* **56** 1601
[24] Weber W 1977 *Phys. Rev.* B **15** 4789
[25] Rustagi K C and Weber W 1976 *Solid State Commun.* **18** 673
[26] Jackson J D 1975 *Classical Electrodynamics* (New York: Wiley)
[27] Rytov S M 1956 *Sov. Phys.–Acoust.* **2** 68
[28] Castrillo P, Colombo L and Armelles G 1994 *Phys. Rev.* B **49** 10 362
[29] Rajput B D 1996 *PhD Thesis*
[30] Nakayama M, Kubota K, Kato H, Chika S and Sano N 1985 *Solid State Commun.* **53** 493
[31] Merlin R, Colvard C, Klein M V, Morkoc H, Cho A Y and Gossard A C 1980 *Appl. Phys. Lett.* **36** 43
[32] Kliewer K L and Fuchs R 1965 *Phys. Rev.* **140** A2076
[33] Zucker J E, Pinczuk A, Chemla D S, Gossard A and Wiegmann W 1984 *Phys. Rev. Lett.* **53** 1280
[34] Kunc K, Balkanski M and Nusimovici M A 1975 *Phys. Status. Solidi* b **72** 229
[35] Grynberg M, Le Toullec R and Balkanski M 1974 *Phys. Rev.* B **9** 517